X-ray Crystallographic Studies of a Series of Penicillin-Derived Asymmetric Inhibitors of HIV-1 Protease‡

Harren Jhoti,* Onkar M. P. Singh, Malcolm P. Weir, Robert Cooke, Peter Murray-Rust, and Alan Wonacott

Department of Biomolecular Structure, Glaxo Research & Development Limited, Greenford, Middlesex, UB6 0HE, England

Received September 9, 1993; Revised Manuscript Received March 30, 1994®

ABSTRACT: In the development of a treatment for AIDS, the HIV-1 protease has been identified as a good target enzyme for inhibitor design. We previously reported a series of dimeric penicillin-derived C_2-symmetric HIV-1 protease inhibitors [Humber, D., *et al.* (1993) *J. Med. Chem. 36*, 3120–3128]. In an attempt to reduce the size and optimize the binding of these C_2-symmetric inhibitors, molecular modeling studies led to a novel series of monomeric penicillin-derived inhibitors of HIV-1 protease. The binding modes of these monomeric inhibitors have been characterized by X-ray crystallographic and NMR studies. Crystal structures of HIV-1 protease complexed to three inhibitors (GR123976, GR126045, and GR137615) from this series identify the molecular details of the interactions. The binding of GR123976 (IC_{50} = 2.3 μM) exhibits good hydrophobic contacts but few electrostatic interactions. A strategy of structure-based design and chemical synthesis led to the elaboration of GR123976 to optimize interactions with the protein. Crystallographic analysis of HIV-1 protease complexed to GR126045 and GR137615 identified these interactions with the catalytic aspartates and the protein binding pockets. The crystal structures of the three complexes confirm the presence of the major interactions modeled in order to optimize potency and reveal details of the molecular recognition by HIV-1 protease of this novel series of nonpeptidic inhibitors.

The function of the aspartic protease of human immunodeficiency virus type 1 (HIV-1[1]) is to cleave the viral *gag* and *gag-pol* polyproteins during the replication cycle of the virus (Krausslich & Wimmer, 1988). It has been shown using site-directed mutagenesis, and also by the use of specific inhibitors of HIV-1 protease, that disruption of this function produces morphologically immature and noninfectious viral particles (Kohl *et al.*, 1988). Thus, HIV-1 protease (HIVP) represents an important therapeutic target in the development of treatment for acquired immunodeficiency syndrome (AIDS).

Several strategies for the development of HIVP inhibitors have been employed. Many of these utilize substrate-based inhibitor design in which the scissile bond has been replaced with a noncleavable isostere, e.g., reduced amide (Billich *et al.*, 1988), hydroxyethylene (Rich *et al.*, 1990), or hydroxyethylamine (Vacca *et al.*, 1991). Other transition-state mimetics such as statine analogues, phosphinates, and difluoro ketone derivatives have also been incorporated into HIVP inhibitors [for reviews, see Huff (1991) and Martin (1992)]. The molecular interactions of many of these types of inhibitors have been identified using X-ray crystallographic and molecular modeling techniques (Wlodawer & Erickson, 1993). These studies have allowed the optimization of lead compounds through an iterative cycle of protein crystallography, biological assays, and medicinal chemistry. Although this approach has resulted in potent HIV-1 protease inhibitors, the high molecular weight and peptidic nature of many of these compounds may be responsible for their generally poor pharmacokinetic properties.

The X-ray crystal structure of HIV-1 protease shows the enzyme to consist of a C_2-symmetric homodimer, with the binding groove lying perpendicular to the 2-fold symmetry axis (Navia *et al.*, 1989; Wlodawer *et al.*, 1989; Lapatto *et al.*, 1989). Strategies that exploit the enzyme structure more directly and use the element of symmetry in the design and synthesis of HIV-1 protease inhibitors have also been pursued. Elegant design experiments using this approach have resulted in C_2-symmetric inhibitors that are potent and specific for HIV-1 protease (Erickson *et al.*, 1990; Kempf *et al.*, 1990).

An alternative to the substrate-based inhibitor design strategy is to use enzyme-based high-throughput screening programs to identify novel lead compounds. We have used this approach to identify a novel series of penicillin-derived C_2-symmetric inhibitors of HIV-1 protease (Humber *et al.*, 1992a, 1993). Structural studies were undertaken to identify the mode of binding of these dimeric C_2-symmetric inhibitors. An X-ray crystal structure of HIV-1 protease complexed with one of these C_2-symmetric dimers, GR116624, exhibited a symmetric binding mode (Figure 1). Subsequent crystallographic studies with other members of this series provided further details of molecular interactions between protein and inhibitor, which were utilized in the synthesis of analogues (Wonacott *et al.*, 1993[2]; Humber *et al.*, 1993).

From the structure–activity relationships (SAR) of this dimer series of penicillin-derived C_2-symmetric inhibitors, it became apparent that optimization of the linker region for interaction with the catalytic aspartates may require the removal of the second penicillin unit (Humber *et al.*, 1993; Holmes *et al.*, 1993a). This would also reduce the inhibitor size, and it was hoped that it might improve the poor pharmacokinetic properties of the C_2-symmetric dimer series.

‡ Coordinates have been deposited in the Brookhaven Protein Data Bank under file names 1HTE, 1HTF, and 1HTG.

* Corresponding author.

® Abstract published in *Advance ACS Abstracts*, June 1, 1994.

[1] Abbreviations: AIDS, acquired immunodeficiency syndrome; HIV-1, human immunodeficiency virus type 1; SAR, structure–activity relationships; HIVP, HIV-1 protease; DMSO, dimethyl sulfoxide; MES, 2-morpholinoethanesulfonic acid; EDTA, ethylenediaminetetraacetic acid; DTT, dithiothreitol; IC_{50}, inhibitor concentration required for 50% inhibition of HIVP using assay conditions reported by Humber *et al.* (1993).

[2] For the purposes of cross-reference, the crystal structures of HIVP/inhibitor complexes referred to by Wonacott *et al.* (1993) as **1**, **2**, and **3** contain inhibitors GR116624, GR122505, and GR127370, respectively.

0006-2960/94/0433-8417$04.50/0

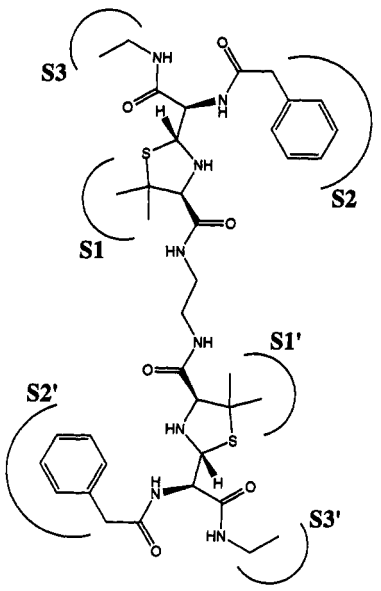

FIGURE 1: Schematic diagram showing the bound conformation of GR116624, a penicillin-derived C_2-symmetric dimer, viewed from the flaps. The binding mode utilizes the S/S′ pockets of the protein and exhibits 2-fold symmetry.

As a result, a series of penicillin-derived monomers was synthesized (Holmes *et al.*, 1993b) on the basis of analysis of the crystal structure of the HIVP/MVT-101 complex (Miller *et al.*, 1989). This structure-based design strategy led to the optimization of potency against HIV-1 protease of early lead compounds, resulting in GR137615 (IC_{50} = 3.8 nM) as described by Holmes *et al.* (1993b) (Table 1). Here we describe the use of X-ray crystallographic and NMR studies, which established the binding mode of key compounds in this series. This study confirms the formation of major interactions designed to optimize potency (Holmes *et al.*, 1993b) and, furthermore, shows in detail the molecular basis for recognition of these nonpeptide inhibitors by HIV-1 protease.

EXPERIMENTAL PROCEDURES

Protein Purification and Crystallization. Recombinant HIV-1 protease was purified following a protocol reported previously (Singh *et al.*, 1991). In each case, the inhibitors were dissolved in 250 μL of DMSO before being added to the enzyme solution. The resulting molar ratio was 10:1, i.e., 10 inhibitor molecules to 1 enzyme dimer. The protein/inhibitor complex was dialyzed for 3 h against 50 mM MES buffer (pH 5.0) containing 1 mM EDTA, 5 mM DTT, and 1 mM sodium azide at 4 °C. Following dialysis, a similar addition of inhibitor was made to maintain the 10:1 inhibitor/protein molar ratio, and the mixture was concentrated to near 4 mg/mL using Amicon YM-10 membranes (Millipore Limited). All chemicals were purchased from Sigma, U.K.

Protein crystallization experiments were set up using the hanging drop vapor diffusion method. Similar conditions were used to crystallize the three complexes; protein concentration was about 4 mg/mL with a 10-fold molar excess of inhibitor, ammonium sulfate (250–500 mM), 50 mM MES, or acetate buffer, the pH ranged between 3.4 and 5.4, and temperatures of 4 and 20 °C were used. All crystals grew to suitable size for X-ray diffraction studies within 7–10 days. The crystals were characterized, and the data are shown in Table 2.

The chemical synthesis of GR123976 has been reported previously (Herak *et al.*, 1978). The flouro analogues used in NMR studies were synthesized following procedures

Table 1: Structure–Activity Relationships of Key Compounds from the Penicillin-Derived Monomer Series Used in This Study

compd	IC_{50} (nM)[a]
GR123976	2265
GR126045	148
GR137615	3.8

[a] The IC_{50} values are taken from Holmes *et al.* (1993).

Table 2: Crystal Characteristics for the HIV-1 Protease/Inhibitor Complexes

inhibitor	space group	unit cell (Å)	resolution (Å)
GR123976 complex **1**	$P2_12_12$	$a = 58.3, b = 87.3, c = 46.4$ $\alpha = \beta = \gamma = 90°$	2.8
GR126045 complex **2**	$P6_1$	$a = b = 63.5, c = 83.2$ $\alpha = \beta = 90°, \gamma = 120°$	2.2
GR137615 complex **3**	$P2_12_12$	$a = 59.3, b = 87.4, c = 46.6$ $\alpha = \beta = \gamma = 90°$	2.0

described elsewhere (Humber *et al.*, 1992b; Kitchin *et al.*, 1993). Synthetic details for the other compounds have been described by Holmes *et al.* (1993b).

Data Collection and Structure Solution. X-ray data for complex **2** were collected on station 9.6 at Daresbury Laboratory (Warrington, U.K.) using the FAST area detector system and a wavelength of 0.89 Å. Diffraction data for complexes **1** and **3** were collected on the in-house FAST area detector system mounted on an Enraf-Nonius FR581 rotating anode. In each case only one crystal was used, and two scans were collected about different axes in the crystal in an attempt to obtain complete data sets. Processing of X-ray intensities was performed using the MADNES (Messerschmidt *et al.*, 1987) software package and then scaled and merged with the CCP4 (CCP4) suite of programs. Data processing statistics for each data set are given in Table 3.

For complex **2**, the crystal form was isomorphous with the first HIV-1 protease complex (GR116624) to be solved in our laboratory (Wonacott *et al.*, 1993). Thus, the protein model from HIVP/GR116624 was used for phasing the initial $(|F_o| - |F_c|)\alpha_{calc}$ map, which showed strong electron density at the active site for the compound. Both complexes **1** and **3** produced

Table 3: Statistics for Data Processing and Refinement for Each Complex[a]

inhibitor	crystal size (μM)	completeness of data (%)	unique reflections	R_{merge} (%)	rms error bonds (Å) angles (deg)	R-factor (%)	resolution (Å)
complex 1	250 × 175 × 25	97	5932	11.2	0.019 3.7	18.9	2.8
complex 2	40 × 40 × 500	95 (87)	4546 (8469)	8.8 (7.7)	0.016 3.0	19.3	2.2
complex 3	315 × 130 × 70	88	14219	7.4	0.016 3.0	19.0	2.0

[a] The numbers in parentheses for complex 2 are for processing the data set in space group $P6_1$.

crystals that belonged to the space group $P2_12_12$, and they were shown to be isomorphous with another of our earlier complexes, HIVP/GR127370, a C_2-symmetric inhibitor (Wonacott *et al.*, 1993). Again, no separate structure determination was required, and initial difference Fourier map calculations for both of these complexes showed strong electron density at the active site.

Refinement and Interpretation. All refinement was performed using X-PLOR (Brunger *et al.*, 1987) and manual adjustments of the structures by using an Evans and Sutherland PS390 graphics system running FRODO (Jones, 1985). Electron density maps were calculated using CCP4 or X-PLOR. The inclusion of water molecules in each structure was based on good electron density and favorable hydrogen-bonding interactions with other atoms. The inhibitor models were built using the graphics program QUANTA (Molecular Simulations Inc., Waltham, MA) running on a Silicon Graphics 4D/35TG workstation.

Interpretation of electron density at the active site for HIVP/inhibitor complexes has been reported, in some cases, to be nontrivial (Murphy *et al.*, 1992). In the case of asymmetric inhibitors, complications can arise due to retrobinding, which results in diffuse or pseudosymmetric electron density. In other cases, the high-symmetry hexagonal space group, $P6_122$, to which some crystals of HIVP/inhibitor complexes belong, introduces a crystallographic 2-fold axis into the active site. This results in electron density with symmetric character, even if the inhibitor is asymmetric and binds in a unique orientation [see Wlodawer and Erickson (1993) and references therein]. For crystals of complex **2**, the initial difference Fourier maps indicated 2-fold-symmetric density at the active site. Although these crystals were treated as belonging to space group $P6_1$, a higher symmetry space group was also considered (see below). Refinement of the complex **2** structure was performed in space group $P6_1$ with GR126045 built into both orientations. The occupancy for each inhibitor model was set to 0.5, and nonbonded interactions between them were turned off in X-PLOR. Conjugate gradient positional refinement cycles were followed by individual *B*-factor refinement and alternated with manual adjustments to the model.

Crystals of both complexes **1** and **3** belong to the orthorhombic space group $P2_12_12$, and as such the inhibitor electron density was not complicated by a crystallographic 2-fold symmetry. The initial difference Fourier map for complex **1** was consistent with the occupation of one side of the active site with GR123976. However, there were also strong electron density features on the opposing side that could not be accounted for by the inhibitor. This density initially was left unexplained, and the inhibitor was modeled into only one side of the active site. Cycles of conjugate gradient refinement together with individual *B*-factor refinement were then performed, after which attempts to interpret the density in the other side of the active site were made as preliminary modeling of the density using another inhibitor molecule proved unsatisfactory. The density features appeared to be consistent with the presence of a peptide, although the nature of the side chains was not clear. A peptide with the sequence Leu-Gln-Glu-Ser was constructed on the basis of the density and known substrate specificity of HIV-1 protease (Poorman *et al.*, 1991), and this peptide also allowed the most favorable H-bonding pattern with the protein. This peptide was then modeled into the density, and further cycles of positional refinement together with individual *B*-factor refinement were performed.

An example of an asymmetric inhibitor binding in two orientations was observed in complex **3**. The initial difference Fourier map at the active site exhibited 2-fold pseudosymmetry suggesting retrobinding of GR137615, and was difficult to interpret due to the overlap of atoms from the two inhibitor orientations. Therefore, initial positional refinement cycles were restricted to the protein and solvent atoms in order to obtain the best possible difference Fourier map for modeling of the inhibitor molecules. For refinement of the inhibitor, both orientations were modeled, as for complex **2**, and the nonbonded interactions between the two inhibitor models were turned off in X-PLOR. The occupancy for each inhibitor model was fixed at 0.5, before further cycles of conjugate gradient positional refinement and individual *B*-factor refinement were performed. During the later stages of refinement, the *B*-factors for each of the two inhibitor orientations were allowed to refine. As with the other structures, manual adjustments of the model and inclusion of waters were alternated with refinement cycles. The difference Fourier maps calculated after this refinement indicated a good fit for both inhibitor models, but the position of the benzimidazole group remained unclear due to overlapping density features (see Figure 2c). In an attempt to clarify the position of this group, a cycle of refinement by simulated annealing (SA) was employed. The model used for this cycle of SA consisted of both inhibitor molecules (one for each orientation), the protein, and solvent molecules. Each inhibitor model was assigned an occupancy of 0.5 before the SA refinement cycle. The slow-cooling SA protocol (Brunger *et al.*, 1987) was used with a starting temperature of 3000 K and a final temperature of 300 K. Following the simulated annealing stage, 120 cycles of conjugate gradient positional refinement were performed before the final cycles of individual *B*-factor refinement. Difference Fourier maps were then calculated, omitting each of the two inhibitor models in turn to confirm that there was good continuous electron density for the two separate orientations (see Figure 3). Thus, the difference Fourier maps shown in Figure 3 were calculated after the SA refinement cycle and omission of the inhibitor molecule actually displayed in the electron density from the map calculation (Figure 3). The quality of the electron density in these maps was much improved and defined both inhibitor conformations more completely by identifying the location of the benzimidazole group. Refinement statistics for each of the HIVP/inhibitor

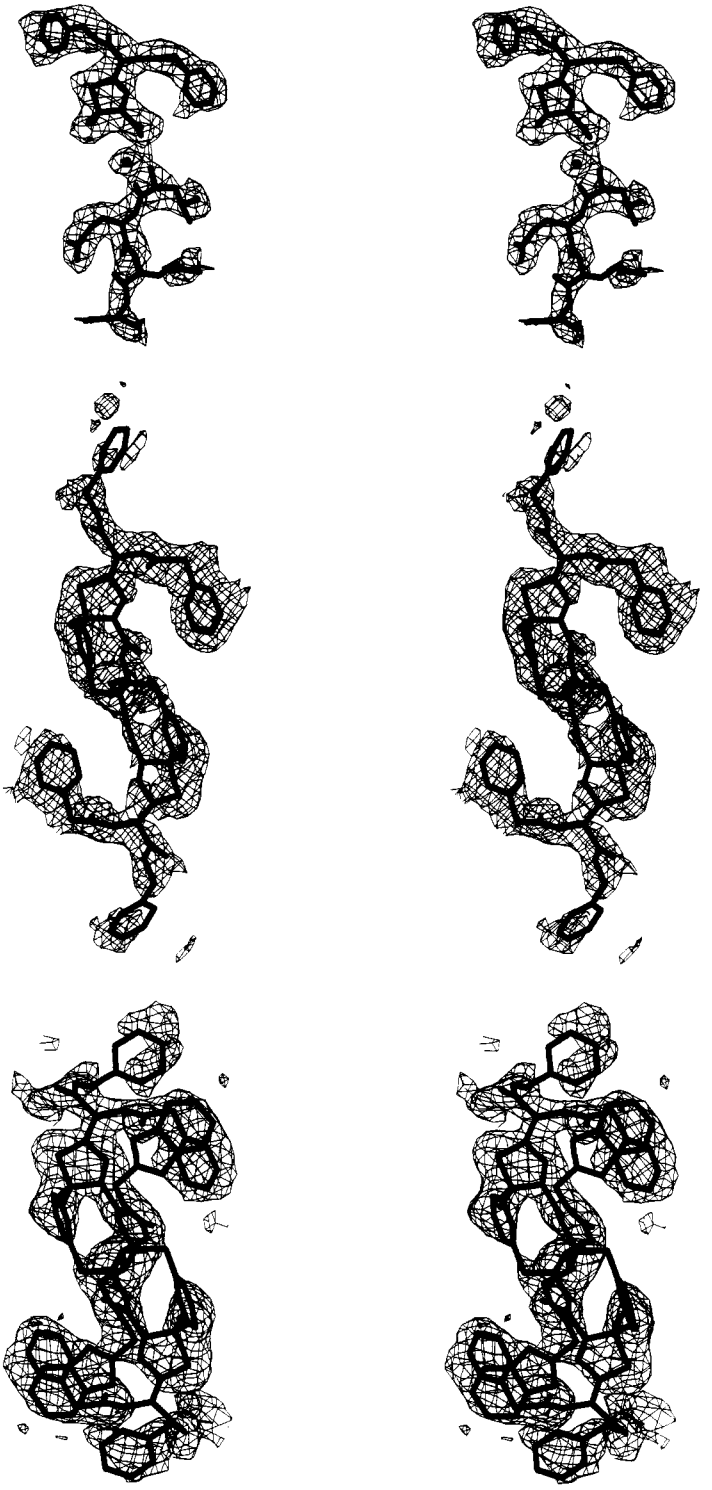

FIGURE 2: Stereodiagrams of difference electron density maps calculated after refinement for each inhibitor, in a similar view as in Figure 1. Each map calculation was performed by omitting the inhibitor models shown in the figure, and the contour level is 1.8σ in each case. (a, top) The electron density for complex **1** suggests that GR123976 binds to one side of the active site. The remaining density (lower half) is consistent with a bound peptide (see text). (b, middle) GR126045 bound in 2-fold related alternate orientations. The binding mode is similar to that observed for complex **1**, but the density for the P3 substituent of GR126045 is weak. (c, bottom) The pseudosymmetric electron density confirms that GR137615 also binds in two alternate orientations. This results in overlapping density features in the S1/S1′ and S2/S2′ binding pockets. The connectivity of density for the nonoverlapping regions only becomes apparent at the 1.0σ contour level. The density for the benzyl ring of the P3 substituent of GR137615 is weak.

complexes are provided in Table 3 and indicate good stereochemistry for the protein/inhibitor models.

NMR Spectroscopy. Solution NMR experiments were performed on samples that were inhibited and concentrated as described above, with additional dialysis into 10 mM acetate-d_3 in D_2O at pH 5.0. Protein concentrations ranged from 2 to 4 mg/mL, and ^{19}F spectra were recorded on a Varian VXR 400-MHz spectrometer at 298 K. Deuterated chemicals were purchased from Aldrich, U.K.

RESULTS

To investigate the overall binding mode of the penicillin-derived monomer series of inhibitors to HIV-1 protease, a fluorinated analogue, GR131598, was used in solution-state

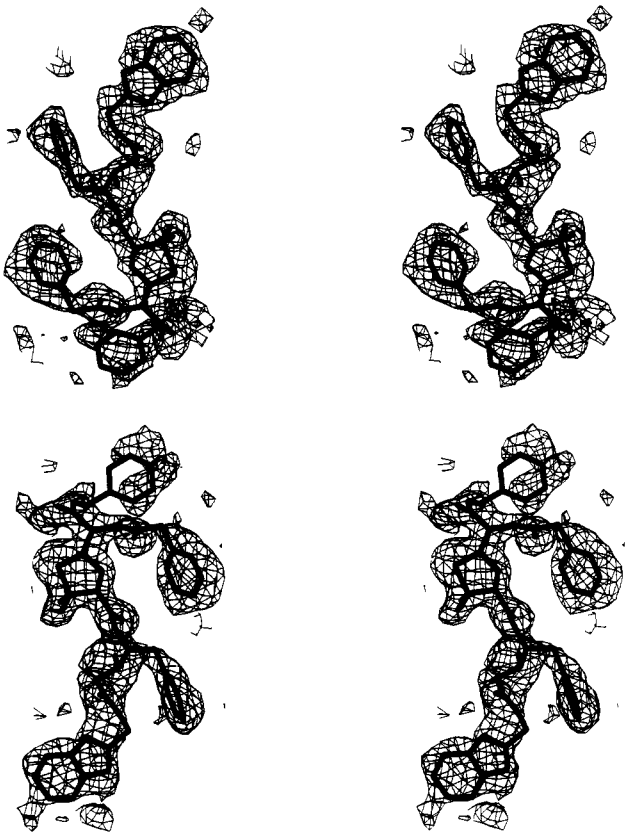

FIGURE 3: Difference electron density maps calculated for complex **3**, with each of the two alternative orientations for GR137615 omitted in turn. In each case the density closely matches the omitted inhibitor model, which is superimposed. The view is similar to that in Figure 2, and the map is contoured at 1.8σ. The connectivity for GR137615 is much improved (cf. Figure 2c), allowing a more complete description of the inhibitor conformation. The benzyl ring of the P3 substituent appears to be disordered.

NMR studies. We have previously employed NMR techniques to establish that the binding mode of the dimeric C_2-symmetric HIVP inhibitors was indeed symmetric (Wonacott *et al.*, 1993). Solution-state ^{19}F NMR studies of GR131598 (an analogue of GR126045) demonstrated a resonance shift upon binding similar to that observed for the corresponding dimeric inhibitor (Figure 4). This result strongly suggested that the monomeric penicillin-derived inhibitors were binding to HIV-1 protease in solution in an equivalent manner to one half of a dimeric C_2-symmetric penicillin-derived inhibitor since the ^{19}F chemical shift is highly sensitive to the environment (Gerig, 1989). To identify the precise binding mode of this series of inhibitors and provide molecular details of the interactions, the crystal structures of complexes **1**, **2**, and **3** were determined.

The overall conformation of the protein is closely similar in all three HIVP/inhibitor complex crystal structures, with the two flaps closed over the active site, thus exhibiting the bound form of the enzyme. This close similarity is highlighted by the superposition of the main chain atoms of the protein in complex **1** and complex **3** (an rms deviation of 0.38 Å for 790 pairs of atoms). The HIV-1 protease consists of a homodimer, and for ease of reference, the two monomers A and B have been numbered 1–99 and 101–199, respectively. The bound conformations of the inhibitors are shown in Figure 2, together with the difference electron density calculated after refinement.

In complex **1** the inhibitor clearly can be seen to bind to only one side of the active site, the other side being occupied by a peptide (Figure 2a). The overall binding mode of the inhibitor is similar to that of the dimer GR116624 (Figure 1), in that the thiazolidine substituent occupies the S1 pocket and the phenylacetate side chain bends back into the S2 pocket. However, there does appear to be a slight but significant difference in the positions of these substituents with respect to the binding pockets for these two inhibitors (Figure 5). Furthermore, in complex **1** the S3 pocket is occupied by the benzyl group, as defined by strong electron density in this region, and the corresponding group in GR116624 is an ethylamine (Wonacott *et al.*, 1993). The S1 binding pocket is well occupied by the thiazolidine group, and in particular the *gem*-dimethyls, which makes good van der Waals interactions with residues Leu123, Ile184, Gly49, Pro181, and Val182. The other hydrophobic binding pocket, S2, is lined by residues Ile47, Val32, Ile84, and Ala 28, and these are in close contact with the phenylacetate side chain. Although the S3 pocket is less well defined and is partly accessible to solvent, it also exhibits some hydrophobic character; the side chains of residues Val182, Leu110, and Arg108 make van der Waals interactions with the benzyl group that occupies this pocket. The guanidinium group of Arg108 is still involved in the intermonomer salt bridge with Asp29, as seen in other HIVP/inhibitor structures (Swain *et al.*, 1990; Wonacott *et al.*, 1993), but in addition it helps to shield the benzyl group of GR123976 from solvent. A more detailed view of the H-bonding interactions between protein and inhibitor is provided in Figure 6.

There appears to be no direct interaction between GR123976 and the catalytic aspartates (Asp25 and Asp125); however, an indirect interaction via a water molecule appears likely. A strong positive density peak between the catalytic aspartates was observed, and although at this resolution a clear identification is difficult, it was interpreted as a water molecule; however, it is also possible that it may be a cation. This water (Wat300) is positioned asymmetrically between the aspartates: it H bonds strongly with Asp125 (2.5 Å), but is more than 3 Å away from Asp 25. This is reminiscent of the water molecule found at a similar position in crystal structures of uncomplexed fungal aspartyl proteases (James & Sielecki, 1983), as well as in the native HIV-1 protease crystal structure (Wlodawer *et al.*, 1989). The carboxylate group of the inhibitor H bonds to this water and thus interacts with the catalytic aspartates; the distance between the carboxylate O4 atom and the water is 2.8 Å (see Figure 6). Furthermore, GR123976 makes only one direct H bond to the protein; the distance from Asp29 amide N to C=O of the phenylacetate side chain is 3.1 Å. The carboxylate of GR123976 also makes an H bond to Wat301 (2.4 Å), which is itself involved in further H bond interactions with the amide nitrogens of Ile50 and Ile150 from the flaps. This water molecule (Wat301) is known to have a crucial role in mediating protein/inhibitor interactions (Miller *et al.*, 1989; Dreyer *et al.*, 1993) and is present in all three structures.

As described previously, electron density is also observed in the other half of the HIV-1 protease active site, which was only interpretable as a bound peptide. Several sequences were attempted when modeling this electron density, including sequences derived from HIV-1 protease; however, the best agreement based on electron density and subsite specificity was Leu-Gln-Glu-Ser (Poorman *et al.*, 1991). As this sequence is not found in HIV-1 protease, the most probable origin of this peptide is from the proteolysis of host cell proteins, during

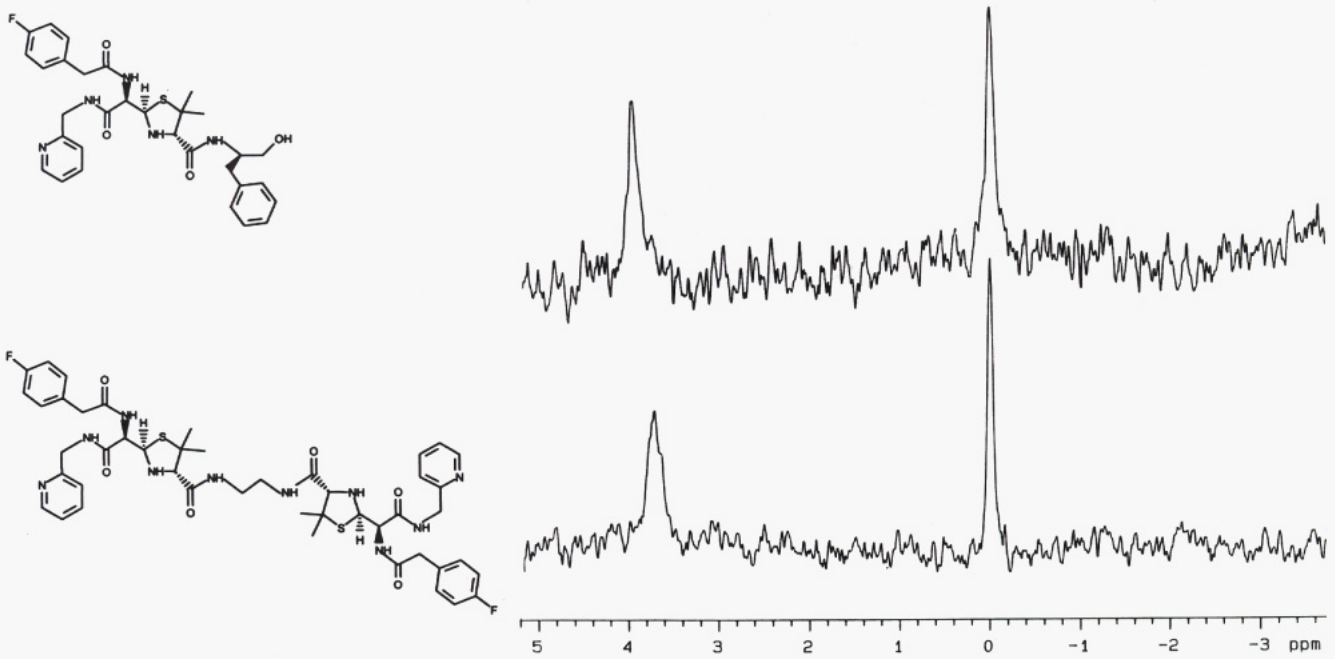

FIGURE 4: NMR spectrum for GR131598 (top), an analogue of GR126045, shows peaks similar to those for an inhibitor from the C_2-symmetric dimer series (bottom). This is indicative of the monomeric penicillin-derived inhibitors binding in a equivalent manner to one half of a dimeric C_2-symmetric inhibitor.

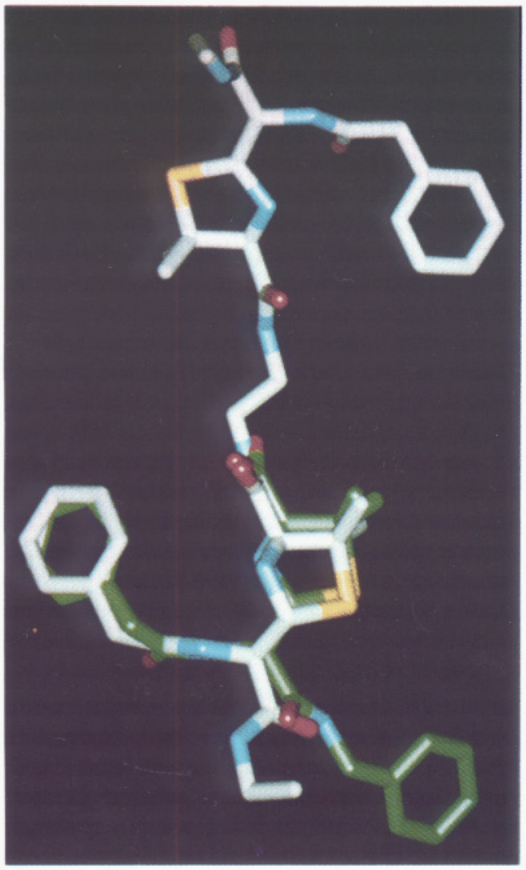

FIGURE 5: Superposition of the bound conformations of GR116624, a C_2-symmetric dimer, with the monomeric GR123976 (green). The overall binding mode is similar, as highlighted by the relative positions of the carbonyls; however, there does appear to be slight shift in the position of GR123976 relative to GR116624, which has consequences for H-bonding interactions (see text).

the expression stage. The conformation of the peptide and its interactions with the protein are shown in Figure 6. Electron density for the peptide backbone is continuous and the P1 and P2 side chains seem ordered, whereas the Glu side chain at P3 has little density as does the Ser at P4 (Figure 2a). Furthermore, the peptide makes good H bonds with the protein; in particular, an H bond from the P1 carbonyl to Wat301 completes the tetrahedral coordination around this water molecule. The amino terminus of the peptide is bound closely to the catalytic aspartates; the NH_2 is about 2.4 Å from the Wat300. A direct interaction between the amino terminus of the peptide and the carboxylate of GR123976 is likely as the inhibitor O4 atom is 2.4 Å from the NH_2 of the peptide. This interaction may help explain the observation that the analogue of GR123976 in which the carboxylate group is replaced by an amide is effectively inactive against HIV-1 protease (Holmes *et al.*, 1993b). Other H bonds between the peptide and the protein include P2 amide N to C=O of Gly127 (3.2 Å), P2 C=O to amide N of Asp129 (2.7 Å), and P3 NH to C=O of Gly148 (3.3 Å). Although the interpretation of this region is tentative due to the lack of resolution, the density features, as well as the resulting interactions, seem consistent with the presence of a peptide. The peptide may have been bound during the purification stage and not displaced, as GR123976 is a relatively weak inhibitor; indeed, similar density has been observed with other weak HIVP inhibitors (T. Skarzynski, unpublished results).

Due to the limited electrostatic interactions between protein and inhibitor in complex **1**, the main contribution to the binding may originate from van der Waals interactions. However, the presence of a water molecule, or a cation, may result in an indirect interaction with the catalytic aspartates, as well as a putative interaction with a bound peptide (see above). The lack of a second penicillin unit presumably allows the hydrophobic substituents of GR123976 to occupy the protein binding pockets optimally. The amount of constraint imposed on the binding of the penicillin-derived inhibitors by a second penicillin unit is indicated by the superposition of the bound conformations of GR123976 and GR116624 (Figure 5). Thus, the structure of the HIVP/GR123976 complex exhibits unrestrained binding of a monomeric penicillin-derived inhibitor with one half of the protein active site. This provides a good structural framework to exploit interaction with the

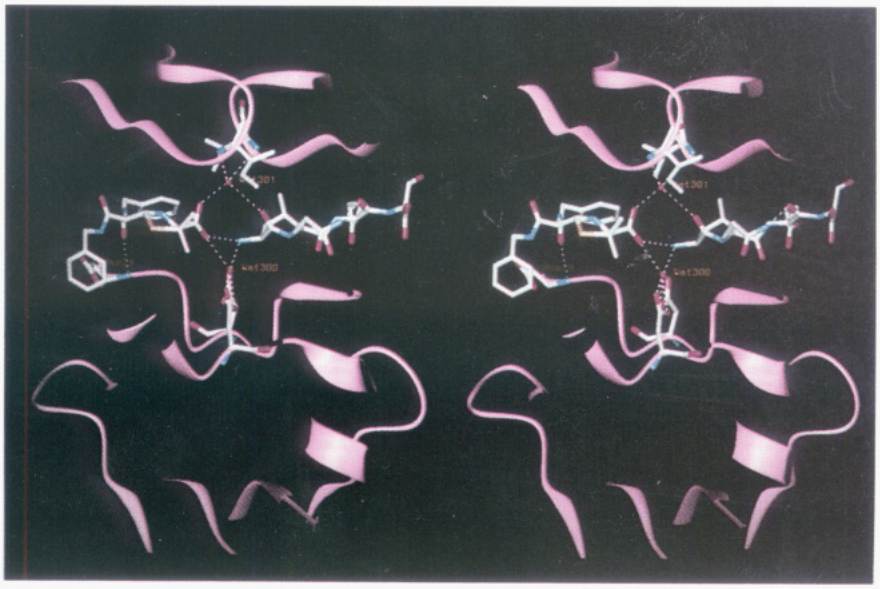

FIGURE 6: Stereoview of the H-bonding interactions observed in complex **1** between the peptide (right), GR123976 (left), and the protein. The backbone of the protein is represented by a ribbon trace with water molecules drawn as red spheres. Also shown is the intrapeptide H bond between the P2 Gln and a peptide carbonyl. The coordination around Wat301 is completed by the amide NH groups of Ile50/150, an inhibitor carboxylate O, and a carbonyl O from the peptide. The network of H bonds between peptide, inhibitor, and protein around Wat300 indicates a unique mode of interaction observed in HIVP.

catalytic aspartates as well as the S′ pockets in an attempt to improve potency in this series of compounds; these elaborations are seen in complexes **2** and **3**. In order to exploit the potentially favorable interaction with the catalytic aspartates (Asp25/Asp125), and also to attempt to occupy the S1′ pocket, analogues bearing a hydroxyl group and an extra lipophilic group were synthesized on the basis of molecular modeling studies (Holmes *et al.*, 1993b). One such compound is GR126045 (Table 1), and its improved potency against HIVP was indicative that the desired interactions had been achieved. To identify precisely the interactions of GR126045 with HIV-1 protease, the crystal structure of complex **2** was determined.

As mentioned above, crystals of complex **2** were characterized as belonging to the hexagonal space group $P6_1$. However, careful inspection of 3-D diffraction data of the *hkn* zones indicated 2-fold symmetry elements. This extra symmetry suggested that the true space group for complex **2** may be $P6_122$. The results of data processing in both space groups $P6_1$ and $P6_122$ are presented in Table 3 and suggest that the higher symmetry space group is also consistent with the data. Alternatively, the 2-fold symmetry elements detected could have arisen due to crystal twinning, as twinned $P6_1$ crystals could give rise to apparent $P6_122$ symmetry. However, we performed the refinement of this structure in $P6_1$, which allowed the explicit incorporation of the entire inhibitor molecule into the active site of the protease dimer, which would not have been possible in $P6_122$. Furthermore, the fidelity of the 2-fold rotational axis that relates the two monomers, which is crystallographic in $P6_122$, could be checked as in $P6_1$ it is noncrystallographic and thus not a constraint. The 2-fold-symmetric nature of the inhibitor electron density (Figure 2b) arises from the asymmetric inhibitor GR126045, exhibiting alternate binding modes. Both orientations were modeled into the density and refined as described above. To assess the intramolecular symmetry of the protease molecule in complex **2**, monomer A was superposed onto monomer B using C^{α} atoms only. A rotation of 179.8° resulted in superposition of the two monomers, with the molecular dyad virtually coincidental with the crystallographic axis. As the refinement for complex **2** was performed in space group $P6_1$, this result indicates that the 2-fold rotational axis relating the monomers is indistinguishable from a true crystallographic rotational axis.

As displayed in Figure 2b, the overall mode of binding of complex **2** is similar to that observed in complex **1**; the thiazolidine ring of GR126045 packs into the S1 pocket, and the phenylacetate side chain occupies the S2 pocket. In addition, strong electron density for the hydroxyl group of GR126045 indicates that a good electrostatic interaction with the Asp25/Asp125 catalytic pair had been achieved. The hydroxyl oxygen atom of GR126045 is located equidistant, about 2.8–3.2 Å, between the oxygen atoms of the two aspartic acid carboxylates (Figure 7). Furthermore, the complex **2** structure shows, as predicted, the binding of a benzyl group into the S1′ pocket. Also present is an electron density peak corresponding to Wat301, which is somewhat surprising as there is only one H bond acceptor from the inhibitor molecule in this region: an amide carbonyl, which provides an H bond to this water molecule (2.8 Å). Indeed, this electron density peak only became apparent in the later map calculations that were based on a well-refined structure. Other electrostatic interactions observed in complex **2** are the H bond between the amide carbonyl of the phenylacetate side chain and the amide N atom of Asp129 (2.8 Å) and also a possible H bond between the NH in the thiazolidine ring and the C=O of Gly148 (3.0 Å) (see Figure 7). This latter H bond was absent from complex **1**, suggesting that although the overall binding has been conserved, there are significant shifts in the positions of the inhibitor substituents in the enzyme pockets.

There appears to be some disorder in the conformation of GR126045, with indistinct electron density for the P3 benzyl ring despite clear density for the amide. The side chain of Arg8/108 exhibits alternate conformations, on the basis of difference Fourier map calculations, and in both cases the intermonomer salt bridge between Arg108/8 and Asp29/129 is disrupted (see Figure 7). In one conformation (binding mode A), the guanidinium group of the arginine residue is rotated away from the aspartic acid into solvent. In the alternative binding mode B, shown in Figure 7, the guanidinium group is moved away, disrupting the salt bridge with the

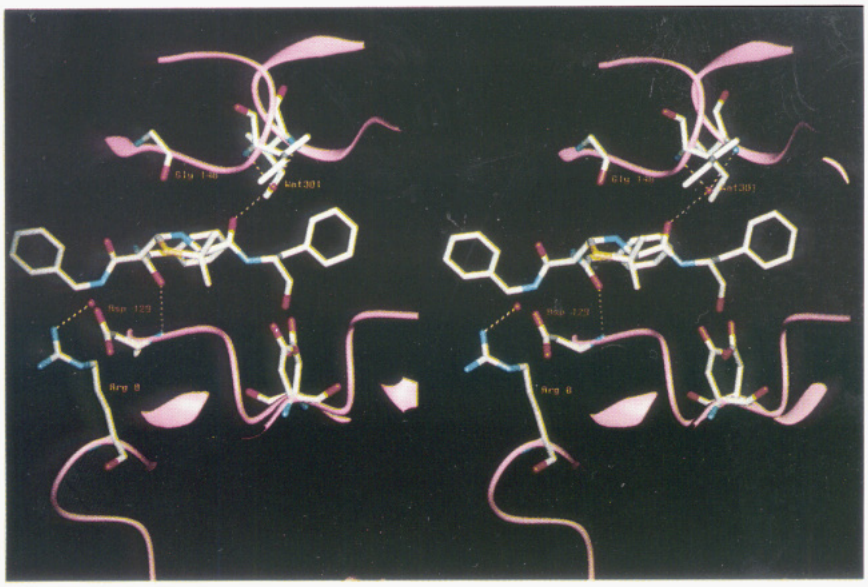

FIGURE 7: Stereoview of complex **2** in a representation similar to that in Figure 6 showing some of the H bonds between inhibitor and protein. For visual clarity, the additional interactions made by GR126045, which include H bonds between the hydroxyl and the catalytic aspartates and also a possible H bond from the thiazolidine NH to Gly148, are not drawn. Incomplete coordination around Wat301 arises from there being only one H bond acceptor in the inhibitor. In this figure, the disrupted intermonomer salt bridge between Arg8/Asp129 is shown as described in binding mode B (see text).

aspartate but this time forming an H bond with a water molecule. Due to steric hindrance, the conformation of the arginine side chain observed in binding mode A is only possible when the S3 pocket is unoccupied, with the inhibitor bound to the opposing half of the active site. Although this is the present interpretation of the disorder observed in the S3 pocket of complex **2**, further refinement with alternate conformations for the Arg8/108 side chain may clarify this situation.

The disruption of this conserved salt bridge is likely to be deleterious to binding. Evidence from SAR of the C_2-symmetric dimer series also suggests that bulky groups in S3/S3′ can result in a decrease in potency against the enzyme (Humber *et al.*, 1993; Wonacott *et al.*, 1993). However, pharmacokinetic considerations for this series of HIV-1 protease inhibitors suggest the requirement of lipophilic groups for cellular potency (Humber *et al.*, 1993). Despite this disorder, it was clear that the binding mode observed in complex **2** displayed the desired extra interactions: good interaction of the inhibitor with the catalytic aspartates and binding of a lipophilic group into the S1′ pocket. This was reflected in the increased potency against HIV-1 protease of GR126045 over GR123976 based on IC_{50} values (Table 1). In an attempt to further improve inhibitor binding, molecular modeling was used to suggest modifications that would improve the interaction with Wat301 by providing an additional H bond acceptor (Holmes *et al.*, 1993b). In addition, it was proposed that binding at the S2′ pocket with a suitable substituent should provide extra favorable interactions. On the basis of this strategy, analogues of GR126045 were synthesized that contained an additional amide and an extra lipophilic group.

This approach led to the synthesis of GR137615, which contains a benzimidazole substituent as well as an additional amide (Table 1). This inhibitor showed improved potency against HIV-1 protease (IC_{50} = 3.8 nM), suggesting an effective binding mode for this series of compounds. Predictions based on the structures of the previous complexes suggested that the benzimidazole group may contribute to this improved binding through specific H bonds to the protein, particularly to the C=O of Gly48/148. To establish the actual binding mode of GR137615, the crystal structure of complex **3** was determined. The initial difference Fourier map calculations exhibited pseudosymmetric electron density for the ligand. This indicated that the asymmetric inhibitor GR137615 was bound to HIV-1 protease in two alternative modes, which were modeled into the density and refined together as described above. The resulting mean *B*-factors for each inhibitor orientation were 26.8 and 29.1 Å^3, suggesting that the distribution between the two orientations was approximately equal. The close match with the mean *B*-factor for the protein backbone (25.8 Å^3) is also consistent with well-defined conformations for the inhibitor models. As expected, complex **3** exhibited occupation of the protein binding pockets similar to that seen in the previous structures. Thus, the thiazolidine ring of GR137615 occupies the S1 pocket, and the phenylacetate side chain occupies the S2 pocket (Figure 2c). For a more detailed description of the binding mode only one of the two inhibitor orientations observed in complex **3** will be discussed, as due to the 2-fold symmetry of the complex these differ very little.

The interaction of GR137615 with the catalytic aspartates (25/125) is effectively the same as in complex **2**: good H bonds are made between the OH and the oxygen atoms of the aspartic acid carboxylates (Figure 8). The thiazolidine ring NH donates an H bond to the backbone carbonyl of Gly48/148, as observed in complex **2**. Also conserved is the H bond between the carbonyl O atom of the inhibitor phenylacetate side chain and the amide N atom of Asp29/129. This interaction is actually one of two H bonds made by the phenylacetate carbonyl; it also H bonds to a buried water molecule (Wat313). This and other H-bonding interactions are shown in Figure 8. The P3 moiety once more displays some disorder with little density present for the benzyl ring. The intermonomer salt bridge between Arg8/108 and Asp29/129 may be weakened due to a possible electrostatic interaction between the benzyl group carbonyl and Arg8/108. Electron density for the additional amide of GR137615 was clear and showed the C=O accepting an H bond from Wat301; the distance between Wat301 and the carbonyl oxygen is 2.7 Å. This H bond completes the tetrahedral coordination of Wat301 and results in an improved interaction in this region of the

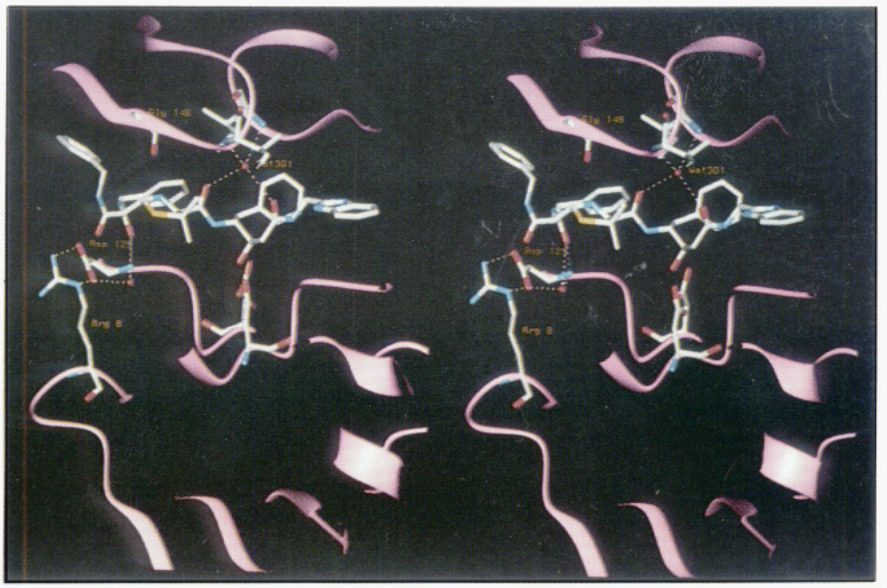

FIGURE 8: In this stereoview of complex **3**, the H-bonding interactions between GR137615 and protein show a completed coordination of Wat301 due to two carbonyl groups present in the inhibitor. As in Figure 7, the interactions between the inhibitor hydroxyl and the catalytic aspartates, as well as the H bond to Gly148, are not drawn. The H bond between the phenylacetate carbonyl of the inhibitor and Wat313 is shown, as is the intermonomer salt bridge between Arg8/Asp129 (see text). The binding of the benzimidazole group does not involve H-bonding interactions, but is largely hydrophobic.

active site. The most difficult region of the overlapped inhibitor density to interpret was the position of the benzimidazole group, which was only clarified by the calculation of omit maps as described above. It was clear from these electron density maps that the benzimidazole group was actually bound into the S2′ pocket. Furthermore, the major interaction was hydrophobic, and the NH in the ring was not involved in specific H bonds to the protein as had been predicted. It also appeared that due to its size, the benzimidazole group might not be optimal in this position; a smaller hydrophobic group might bind better. Replacement of the benzimidazole group by a phenyl resulted in similar potency against the enzyme (Holmes *et al.*, 1993b).

DISCUSSION

The role of symmetry in the binding of both symmetric and asymmetric inhibitors to HIV-1 protease has been discussed previously (Erickson *et al.*, 1990; Murthy *et al.*, 1992; Wlodawer & Erickson, 1993). In the case of HIVP/inhibitor complexes solved from orthorhombic crystals, where the whole dimer is contained in the asymmetric unit, there are two possibilities: the inhibitor binds in a unique orientation (as in complex **1**) or in alternative binding modes (as in complex **3**). Actually, in the latter case it may be that the enzyme dimer binds the inhibitor in a unique orientation, but then this complex is randomly packed in the crystal. The situation becomes more complex in the case of hexagonal crystals, where a crystallographic 2-fold rotational axis relating the monomers exists, as in $P6_122$. This necessarily introduces disorder into the inhibitor conformation, as the asymmetric unit contains a monomer and only part of the inhibitor. When faced with this problem, most workers (Erickson *et al.*, 1990; Dreyer *et al.*, 1992, 1993), including ourselves, have chosen to perform the crystallographic calculations in $P6_1$, which places the whole complex in the asymmetric unit and allows a realistic interpretation of the inhibitor conformation.

It has been suggested that a prerequisite for HIVP/inhibitor complexes to crystallize in hexagonal space groups is that the overall symmetry of the dimer must not be disrupted (Murthy *et al.*, 1992). This may be satisfied by a (pseudo-) symmetric inhibitor such as A-74704 or SKF108361, and indeed both of these complex to HIV-1 protease and produce hexagonal crystals (Erickson *et al.*, 1990; Dreyer *et al.*, 1993). If the inhibitor is asymmetric in nature but is small enough to be completely enclosed within the active site, hexagonal crystals may still result as the overall symmetry of the complex is preserved. An example of this is observed in the structures of the hydroxyethylene-based inhibitors complexed with HIV-1 protease, as reported by Murthy *et al.* (1992). However, complex **2**, which crystallizes as hexagonal rods, shows a truly asymmetric inhibitor, GR126045, bound to the enzyme, but not enclosed within the active site. Therefore, it seems that the rules that determine the packing arrangements for HIVP/inhibitor complexes in crystals remain unclear. In fact, a common observation is that both hexagonal rodlike and orthorhombic plate crystals grow in the same hanging drop during the crystallization of an HIVP/inhibitor complex. This suggests that there must be only a slight preference for the particular thermodynamically stable packing arrangement.

An estimated 160 crystal structures of HIV-1 protease complexed with inhibitors have been determined in laboratories around the world (Wlodawer & Erickson, 1993). Although most of the published structures are of inhibitors containing peptidomimetics, the HIV-1 protease appears to show a remarkable degree of conservation in its mode of binding. However, an interesting exception is the HIVP/haloperidol analogue complex, where the protein conformation is significantly different from that found in other HIVP/inhibitor complexes (Rutenber *et al.*, 1993). But in general, this conservation of binding has also been shown to extend to nonpeptidic inhibitors, as highlighted in our previous report describing the binding of the penicillin-derived C_2-symmetric inhibitors to HIV-1 protease (Wonacott *et al.*, 1993). In the present study, we observe that the penicillin-derived asymmetric monomers also utilize the substrate binding pockets in HIV-1 protease and, thus, conserve the mode of binding. These observations suggest an inherent adaptability in the binding pockets of HIV-1 protease, allowing the enzyme to bind a variety of chemically distinct substituents using the same residues. This can be visualized by a superposition of the

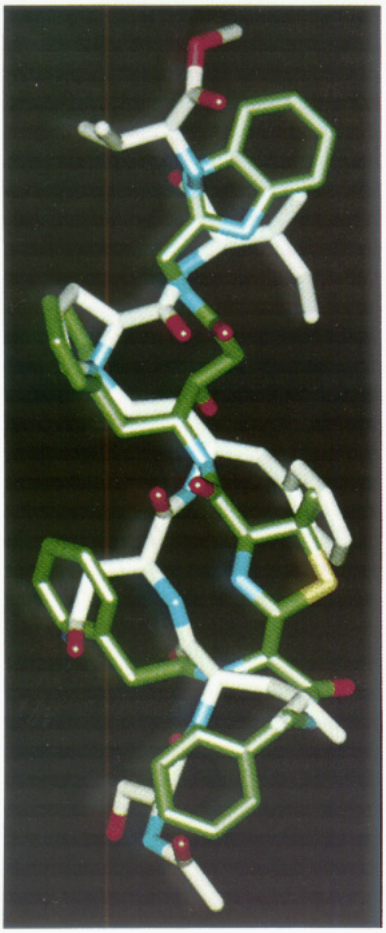

FIGURE 9: Superposition of the bound conformations of JG-365 and GR137615 (green) highlighting the similarities in the modes of binding exhibited by the HIV-1 protease. Although each inhibitor traces a different path through the active site, the protein S/S′ binding pockets are occupied to a similar extent.

bound conformations of GR137615 and JG-365 (Swain *et al.*, 1990), a hydroxyethylamine type inhibitor (Figure 9). Although the trace of each inhibitor backbone through the active site is very different, the substituents in the binding pockets overlay rather well; e.g., the *gem*-dimethyls of GR137615 and the Phe side chain of JG-365 occupy similar space in the S1 pocket.

The crystal structure of complex **1** shows for the first time, as far as we are aware, an HIV-1 protease inhibitor bound only to one side of the active site, with the rest of the site apparently occupied by a peptide. The inhibitor, GR123976, binds in a unique orientation, as implicated by the asymmetric electron density (Figure 2a). Relatively few electrostatic interactions between inhibitor and protein are observed in complex **1**; however, indirect interactions are achieved via ordered water molecules such as Wat301. This water molecule has been observed in almost all HIVP/inhibitor complexes reported so far; interestingly, it has no counterpart in the fungal aspartyl protease/inhibitor complexes (James & Sielecki, 1983; Sugana *et al.*, 1987). It appears to be totally buried and mediates interactions between the inhibitor and the flaps of the protein (Swain *et al.*, 1990; Dreyer, *et al.*, 1992). A tetrahedral coordination around Wat301 is usually achieved by the acceptance of H bonds from the amide nitrogens Ile50/150 from the flaps and the donation of H bonds to appropriate functionalities, usually carbonyl oxygens, in the inhibitor. In complex **1** the *B*-factor of Wat301 is 16 Å^2, which is relatively low when compared with complex **2**, where the *B*-factor of Wat301 is 35 Å^2. This suggests that Wat301 is less tightly bound in complex **2**, in spite of the fact that both inhibitors, GR123976, and GR126045, contain only a single C=O in the correct position for accepting an H bond from Wat301. The apparent inconsistency may be explained if the unaccounted density in the active site of complex **1** is indeed a peptide, which could provide another C=O to complete the tetrahedral coordination of Wat301. Also, in complex **1** the H bond between the inhibitor and Wat301 is likely to be stronger, as it originates from a carboxylate group. Nevertheless, it is clear from the *B*-factors for complex **2** that optimal interaction with Wat301 cannot be achieved with only one H bond acceptor functionality in the inhibitor. This interaction was optimized in complex **3**, as GR137615 contains two C=O groups correctly positioned to fulfill these potential H bonds; the *B*-factor for Wat301 in **3** is 21 Å^2. In terms of improving inhibitor potency, an alternative approach would be to attempt to replace Wat301 with a suitable functionality designed for direct interactions with the flaps. As suggested previously, this could lead to novel and, based on entropic considerations, more potent HIVP inhibitors (Wlodawer & Erickson, 1993).

Analogues of statine that mimic the transition state have been incorporated into aspartyl protease inhibitors (Fischer, 1988; Huff, 1991). In these analogues, the stereochemistry is *S* at the asymmetric center, which bears the lipophilic group P1. The peptide isostere contained in GR137615 is structurally related to statine, but here the asymmetric center has *R* stereochemistry, and also the lipophilic group actually binds in the S1′ rather than the S1 pocket (Holmes *et al.*, 1993b). Thus, the structure of complex **3** represents a novel binding mode for a statine analogue; i.e., the P1 benzyl group takes a direct and novel path to the S1′ pocket. In particular, the binding of GR137615 to HIV-1 protease represents an effective binding mode, as highlighted by its potency, in this series of inhibitors. Together, the crystal structures of complexes **1**, **2**, and **3** have established the specific interactions involved in the binding of HIV-1 protease to this series of penicillin-derived inhibitors. As such, this study has provided an insight into the molecular basis of recognition by HIV-1 protease of this nonpeptidic series of inhibitors. The use of this structure-based design strategy has resulted in the development of a novel series of penicillin-derived inhibitors that are potent for HIV-1 protease (Holmes *et al.*, 1993b).

ACKNOWLEDGMENT

We thank Dr. Mike Hann and Dr. Peter McMeekin for useful discussions; Dr. Dev Baines for assistance in protein purification; and Dr. Tadeusz Skarzynski for data collection and refinement of complex **1**. We also thank Dr. Richard Bethell, Dr. David Orr, and Mr. Norman Gray for enzyme inhibition data and Mr. Nicholas Nieland and Mr. Nicholas Holliday for synthesis of the fluoro analogues used in the NMR studies.

REFERENCES

Billich, S., Knoop, M.-T., Hansen, J., Strop, P., Sedlacek, J., Mertz, R., & Moelling, K. (1988) *J. Biol. Chem. 263*, 17905–17908.

Brunger, A. T., Kuriyan, J., & Karplus, M. (1987) *Science 235*, 458–460.

CCP4 (The SERC Collaborative computing project No. 4), A suite of programs for Protein Crystallography, Daresbury Laboratory, U.K.

Dreyer, G. B., Lambert, D. M., Meek, T. D., Carr, T. J., Tomaszek, T. A., Jr., Fernandez, A. V., Bartus, H., Cacciavillani, E., Hassell, A. M., Minnich, M., Petteway, S. R., Jr., & Metcalf, B. W. (1992) *Biochemistry 31*, 6646–6659.

Dreyer, G. B., Boehm, J. C., Chenera, B., DesJarlais, R. L., Hassell, A. M., Meek, T. D., Tomaszek, T. A., Jr., & Lewis, M. (1993) *Biochemistry 32*, 937–947.

Erickson, J., Neidhart, D. J., VanDrie, J.; Kempf, D. J., Wang, X. C., Norbeck, D. W., Plattner, J. J., Rittenhouse, J. W., Turon, M., Wideburg, N., Kohlbrenner, W. E., Simmer, R., Helfrich, R., Paul, D. A., & Knigge, M. (1990) *Science 249*, 527–533.

Fischer, G. (1988) *Nat. Prod. Rep.*, 465–495.

Gerig, J. T. (1989) *Methods Enzymol. 177*, 3–23.

Herak, J. J., Kovacevic, M., & Gaspert, B. (1978) *Croat. Chem. Acta 51*, 265–272.

Holmes, D. S., Clemens, I. R., Cobley, K. N., Humber, D. C., Kitchin, J., Orr, D. C., Patel, B., Paternoster, I. L., & Storer, R. (1993a) *Bioorg. Med. Chem. Lett. 3*, 503–508.

Holmes, D. S., Bethell, R. C., Cammack, N., Clemens, I. R., Kitchin, J., McMeekin, P., Mo, C. L., Orr, D. C., Patel, B., Paternoster, I. L., & Storer, R. (1993b) *J. Med. Chem. 36*, 3129–3136.

Huff, J. R. (1991) *J. Med. Chem. 34*, 2305–2314.

Humber, D. C., Cummack, N., Coates, N. J. A. V., Cobley, K. N., Orr, D. C., Storer, R., Weingarten, G. G., & Weir, M. P. (1992a) *J. Med. Chem. 35*, 3080–3081.

Humber, D. C., Weingarten, G. G., Storer, R., Kitchin, J., & Hann, M. M., Glaxo Group Research, Greenford, Middx., U.K. (1992b) Thiazolidine derivatives and their use in therapy, Patent WO92/20665.

Humber, D. C., Bamford, M. J., Bethell, R. C., Cammack, N., Cobley, K., Evans, D. N., Gray, N. M., Hann, M. M., Orr, D. C., Saunders, J., Shenoy, B. E. V., Storer, R., Weingarten, G. G., & Wyatt, P. G. (1993) *J. Med. Chem. 36*, 3120–3128.

James, M. N. G., & Sielecki, A. R. (1983) *J. Mol. Biol. 163*, 299–361.

Jones, A. T. (1985) *Methods Enzymol. 115*, 157–171.

Kempf, D. J., Codacovi, L., Wang, X.-C., Norbeck, D. W., Kohlbrenner, W. E., Wideburg, N. E., Knigge, P. D. A., Vasavanonda, S., Saldivar, A. C. K. A., Rosenbrook, W., Jr., Clement, J. J., Plattner, J. J., & Erickson, J. (1990) *J. Med. Chem. 33*, 2687–2689.

Kitchin, J., Holmes, D. S., Humber, D. C., Storer, R., Hann, M. M., McMeekin, P., Murray-Rust, P., Patel, B., & Weingarten, G. G., Glaxo Group Research Ltd., Greenford, Middx., U.K. (1993) Thiazolidine derivatives and their use as anti-viral compounds, Patent WO93/01174.

Kohl, N. E., Emini, E. A., Schleif, W. A., Davies, L. J., Heimbach, J. C., Dixon, R. A. F., Scholnick, E. M., & Sigal, I. S. (1988) *Proc. Natl. Acad. Sci. U.S.A. 85*, 4686–4690.

Krausslich, H.-G., & Wimmer, E. (1988) *Annu. Rev. Biochem. 57*, 701–754.

Lapatto, R., Blundell, T. L., Hemmings, A., Overington, J., Wilderspin, A., Wood, S., Merson, J. R., Whittle, P. J., Danely, D. E., Geoghegan, K. F., Hawrylik, S. J., Lees, S. E., Scheld, K. G., & Hobart, P. M. (1989) *Nature 342*, 299–302.

Martin, J. A. (1992) *Antiviral Res. 17*, 265–278.

Messerschmidt, A., & Pflugrath, J. W. (1987) *J. Appl. Crystallogr. 20*, 306–315.

Miller, M., Schneider, J., Sathyanarayana, B. K., Toth, M. V., Marshall, G. M., Clawson, L., Selk, L., Kent, S. B. H., & Wlodawer, A. (1989) *Science 246*, 1149–1152.

Murthy, K. H. M., Winborne, E. L., Minnich, M. D., Culp, J. S., & Debouck, C. (1992) *J. Biol. Chem. 267*, 22770–22778.

Navia, M. A., Fitzgerald, P. M. D., McKeever, B. M., Leu, C.-T., Heimbach, J. C., Herber, W. K., Sigal, I. S., Darke, P. L., & Springer, J. P. (1989) *Nature 337*, 615–620.

Poorman, R. A., Tomasselli, A. G., Heinrikson, R. L., & Kezdy, F. J. (1991) *J. Biol. Chem. 266*, 14554–14561.

Rich, D. H., Green, J., Toth, M. V., Marshall, G. R., & Kent, S. B. H. (1990) *J. Med. Chem. 33*, 1285–1288.

Rutenber, E., Fauman, E. B., Keenan, R. J., Fong, S., Furth, P. S., Ortiz de Montellano, P. R., Meng, E., Kuntz, I. D., DeCamp, D. L., Salto, R., Rosé, J. R., Craik, C. S., & Stroud, R. M. (1993) *J. Biol. Chem. 268*, 15343–15346.

Singh, O. M. P., Baines, B. S., Hall, R. M., Gray, N. M., & Weir, M. P. (1991) *J. Biotechnol. 21*, 127–136.

Sugana, K., Padlan, E. A., Smith, C. W., Carlson, W. D., & Davies, D. R. (1987) *Proc. Natl. Acad. Sci. U.S.A. 84*, 7009–7013.

Swain, A. L., Miller, M. M., Green, J., Rich, D. H., Schneider, J., Kent, S. B. H., & Wlodawer, A. (1990) *Proc. Natl. Acad. Sci. U.S.A. 87*, 8805–8809.

Vacca, J. P., Guare, J. P., de Solms, S. J., Sanders, W. M., Giuliani, E. A., Young, S. D., Darke, P. L., Zugay, J., Sigal, I. S., Schleif, W. A., Quintero, J. C., Emini, E. A., Anderson, P. S., & Huff, J. R. (1991) *J. Med. Chem. 34*, 1225–1228.

Wlodawer, A., & Erickson, J. W. (1993) *Annu. Rev. Biochem. 62*, 543–585.

Wlodawer, A., Miller, M., Jaskólski, M., Sathyanarayana, B. K., Baldwin, E., Weber, I. T., Selk, L. M., Clawson, L., Schneider, J., & Kent, S. B. H. (1989) *Science 245*, 616–621.

Wonacott, A., Cooke, R., Hayes, F. R., Hann, M. M., Jhoti, H., McMeekin, P., Mistry, A., Murray-Rust, P., Singh, O. M. P., & Weir, M. P. (1993) *J. Med. Chem. 36*, 3113–3119.